High-Efficiency Conversion of CO_2 to Oxalate in Water is Possible Using a Cr-Ga Oxide Electrocatalyst

Aubrey R. Paris, Andrew B. Bocarsly*

Department of Chemistry, Princeton University, Princeton, New Jersey 08544, United States

ABSTRACT: Electrochemical transformation of CO_2 into commodity chemicals such as oxalate is a strategy for profitably remediating high atmospheric CO_2 levels. Electrocatalysts for oxalate generation, however, have required prohibitively large applied potentials forcing the use of nonaqueous electrolytes. Here, a thin film comprised of alloyed Cr and Ga oxides on glassy carbon is shown to electrocatalytically generate oxalate from aqueous CO_2 with high Faradaic efficiencies at 690 mV overpotential. Oxalate is produced at a surface anion site via a CO-dependent pathway; the process is highly sensitive to the hydrogen bonding environment and avoids the commonly invoked $CO_2^{\bullet-}$ intermediate. Ultimately, this catalytic system accomplishes efficient CO_2-to-oxalate conversion in protic electrolyte.

KEYWORDS: CO_2 reduction, electrocatalyst, oxalate, metal oxide, chromium, gallium, aqueous

1. INTRODUCTION

High atmospheric CO_2 concentrations and associated water security, food access, and public health challenges[1,2] are motivating chemists to develop electrocatalysts capable of transforming CO_2 into value-added fuels or chemical feedstocks.[3] Future use of these technologies could make CO_2 reuse a profitable process, encouraging point-source or atmospheric CO_2 capture while simultaneously helping to achieve emission reduction goals. Industrially attractive electrocatalysts of this sort exhibit several key traits, including the ability to generate a multi-carbon product selectively and efficiently. As such, the two-electron reduction product oxalate is an ideal target because of its small electron requirement coupled with commercial appeal; oxalate is a precursor to glycols,[4,5] which themselves are precursors to a variety of synthetic materials.[6]

The standard redox potentials, E_R°, for CO_2 reduction to oxalic acid, monoanionic oxalate, and dianionic oxalate are only –0.48,[7] –0.52, and –0.64 V vs. NHE, respectively (see Supporting Information), but prior studies have reported that applied potentials of at least –2 V vs. NHE are necessary to achieve the desired transformation at reasonable reaction rates.[8–11] Studies on the reduction of CO_2 to oxalate have typically[12,13] employed organic electrolytes[8,10,11,14–19] to avoid competition with H_2 evolution reactions.[20,21] The need for a nonaqueous solvent, along with a supportive body of kinetic data,[8] has led researchers to assert that oxalate formation occurs through generation of a reactive $CO_2^{\bullet-}$ intermediate.[9,11,22] This conclusion is based, in part, on the fact that the one-electron reduction of CO_2 to form $CO_2^{\bullet-}$ occurs at E_R° = –1.90 V vs. NHE.[23] If oxalate must be formed via this pathway, a minimum effective electrode overpotential of nearly 1.5 V would be required to simply initiate a low rate of conversion. Further, exploration of electrocatalysts for this transformation would be of little value since the best catalyst would still require electrode operation at potentials more negative than –1.90 V vs. NHE.

Here, we report the use of an electrode composed of a Cr_2O_3-Ga_2O_3 alloy thin film (3 Cr_2O_3:1 Ga_2O_3; hereafter referred to as Cr-Ga) on glassy carbon to transform CO_2 to oxalate in aqueous electrolyte at potentials as positive as –0.98 V vs. NHE (–1.18 V vs. Ag/AgCl). Maximum oxalate Faradaic efficiencies of 59% were achieved using pH 4.1 aqueous KCl at –1.48 V vs. Ag/AgCl, an overpotential of only 690 mV. Based on the observed electrode potential alone, generation of a $CO_2^{\bullet-}$ intermediate can be ruled out. Thus, a previously unknown reaction pathway exists which bypasses the one-electron reduction of CO_2, thereby providing a low energy route to forming oxalate during CO_2 electroreduction. To our knowledge, all prior electrocatalyst systems capable of transforming CO_2 to oxalate required a nonprotic environment due to the presence of a $CO_2^{\bullet-}$ intermediate. The reaction pathway presented in this work introduces new possibilities for catalyst discovery and tangible opportunities for the energy-efficient conversion of CO_2 to a multicarbon chemical feedstock.

2. EXPERIMENTAL SECTION

2.1 Materials

Chromium(III) nitrate nonahydrate (≥ 99.99%), gallium(III) nitrate hydrate (99.9%), $KHCO_3$ (99.7%), oxalic acid (≥ 99%), NH_4Cl (99.998%), $(CH_3)_4NCl$ ((TMA)Cl; ≥ 98%), NaCN (97%), methanol (≥ 99.9%), ^{13}C-methanol (99 at% ^{13}C), formic acid (≥ 98%), 1,4-dioxane (99.8%), acetonitrile (99.8%), ethanol (≥ 99.8%), isopropanol (≥ 99.7%), $^{13}CO_2$ (99 at% ^{13}C), ^{12}CO (^{13}C-depleted), and ^{13}CO (99 at% ^{13}C) were obtained from Sigma-Aldrich. KCl, KBr, KI, K_2CO_3, K_2SO_4, KH_2PO_4, LiCl, CsCl, $CaCl_2$, and HCl, all ACS grade, were purchased from EMD Chemicals, and calcium bromide (99.5%) was obtained from Alfa Aesar. Ar, CO_2, CO, 95% Ar/5% H_2, and 50% CO/50% H_2 gases and mixtures were ordered from AirGas. Glassy carbon plates (GLAS11; 25 x 25 x 3 mm; Structure Probe Inc.) were cut in half lengthwise prior to use. Conducting silver and Loctite Hysol insulating epoxies were purchased from Epo-Tek and Grainger,

respectively. All chemicals were used as received except for methanol and formic acid for standard curves, 1,4-dioxane for NMR internal standards, and HCl, all of which were diluted prior to use.

2.2 Cr-Ga thin film synthesis and characterization

Synthetic procedures to create Cr-Ga thin films of various stoichiometries (most commonly 3:1) were adapted from the method established by Torelli *et al.*[23] Briefly, aqueous solutions of 0.052 M chromium(III) nitrate nonahydrate and 0.036 M gallium(III) nitrate hydrate were mixed to achieve the desired Cr:Ga ratio. Glassy carbon pieces were heated to ~120 °C on a hotplate, and 0.1-mL samples of the Cr-Ga nitrate solution were drop-casted onto them. After the solution evaporated completely, the glassy carbon pieces were placed in an alumina boat and loaded into either a Lindberg/Blue M or Carbolite Quartz Tube Furnace. The furnace was ramped at a rate of 3 °C/min to 700 °C under 95% Ar/5% H_2 gas flow; it rested at this state for 5 h prior to cooling to room temperature at a rate of –3 °C/min. Resulting Cr-Ga films (geometric surface area ~0.8 cm^2) were olive green in color, with Cr-rich stoichiometries tending toward Kelly green and Ga-rich stoichiometries tending toward gray.

The compositions and morphologies of Cr-Ga films were analyzed by a variety of materials characterization techniques. Powder X-ray diffraction was performed using a Bruker D8 Advance diffractometer with 0.083° step size and CuKα radiation. XRD samples either remained on the glassy carbon support or were scraped from the surface; resulting patterns were identical, except that scraped samples exhibited significantly less carbon intrusion and were therefore selected for presentation herein. Thin film morphology and additional bulk composition data were obtained using a FEI XL30 FEG-SEM equipped with EVEX EDS detector. SEM images and EDX spectra were obtained using a 5 or 10 keV electron beam with a 10–15 mm working distance. A Titan Cubed Themis 300 Scanning/Transmission Electron Microscope with Super-X EDS detector was used to obtain high-resolution TEM/EDS data. XPS spectra were collected using a ThermoFisher K-Alpha X-Ray Photoelectron Spectrometer set to 20 eV pass energy and 50 ms dwell time. Resulting data were analyzed using the Thermo Scientific Avantage Data System and CasaXPS software.

Materials characterization was conducted before and after electrochemistry in designated experiments. XPS of electrodes after electrolysis indicated that no surface-contaminating components were generated during electrochemical experiments (e.g., Pt from the counter electrode—situated in a separate compartment during electrolysis—or reference electrode species).

2.3 Electrode preparation and electrochemical experimentation

Electrodes were prepared in one of two fashions. One electrode configuration involved connecting copper wire to the glassy carbon support using conducting silver epoxy, feeding the wire through a glass tube, and covering both ends of the tube (including any exposed copper or silver) with insulating epoxy. The second configuration featured the same general setup, but the copper wire was attached to an alligator clip, which could then be used to reversibly hold glassy carbon pieces whose tops had been wrapped in copper tape. Experiments using both electrode configurations yielded identical results, both in terms of charge passage and product distribution.

Electrochemical experiments were conducted using CH Instruments 760 and 1140 potentiostats. Bulk electrolysis experiments utilized custom electrochemical cells with gas-tight ports for the working, Pt mesh counter (situated in a gas dispersion tube), and Ag/AgCl reference electrodes. The electrolyte was continuously stirred. Unless otherwise noted, 0.1 M KCl (5–8 mL) was used as the electrolyte, and it was buffered with $KHCO_3$ to achieve CO_2-saturated pH values > 4 or adjusted with 0.01 M HCl for values < 4. Electrolyte solutions were purged with CO_2 for 30 min prior to experimentation. In experiments without CO_2 (i.e., CO, formic acid, methanol, or combinatorial feedstocks), the pH was adjusted to the appropriate, CO_2-analogous value. The majority of electrolyses were conducted at pH 4.1, and post-electrolysis measurements indicated that the final solution pH was consistently between 4.5 and 5.0. Experiments using $^{13}CO_2$, ^{13}CO, and ^{12}CO (^{13}C-depleted) were not completely purged with the respective gas. Electrolysis experiments were performed until 30–40 C charge had passed, unless the experiment was meant to determine catalyst lifetime.

2.4 Product analysis

The solution and headspace of electrochemical cells were sampled for liquid and gaseous products by ^1H-NMR and gas chromatography, respectively, both during and after bulk electrolysis. Formate and methanol were detected by ^1H-NMR after combining 530 µL electrolyte with 60 µl D_2O and 10 µL 1,4-dioxane (10 mM); the latter served as an internal standard. In ^{13}C-NMR experiments (used primarily to detect oxalate), only 1 µL 1,4-dioxane (10 mM) was added. A Bruker Avance III 500 MHz NMR Spectrometer with cryoprobe detector was used for all NMR experiments, and the experiments incorporated a custom water suppression method to permit sampling of aqueous electrolyte solutions. Formate and methanol were quantified using 5-point calibration curves for ^1H-NMR ($R^2 > 0.99$; detection limit ~ 0.1 µM), while oxalate was visualized qualitatively by a large ^{13}C-NMR signal (in experiments utilizing ^{13}C-labeling) in the 160–170 ppm range.

Oxalate was quantified using the time-honored method of precipitation by a calcium salt.[24] A 2-mL sample of the electrolysis solution was treated with 0.5 mL, 1 M HCl (to remove any carbonate present), and then 1 mL, 1 M calcium bromide solution was added, resulting in the precipitation of calcium oxalate. The calcium oxalate sample was dried in an oven at 105 °C overnight and then weighed; this mass was used to calculate the total quantity of oxalate formed. The limit of detection using this method was determined by isolating known quantities of aqueous oxalate (total electrolysis cell detection limit ~ 0.1 mmol; see Figure S1 for complete details). IR spectra of calcium oxalate samples were obtained using a Thermo Diamond Smart Orbit IR Spectrometer (1 cm^{-1} resolution). The carbonate byproduct could be quantified by finding the difference in mass between two electrolysis samples,

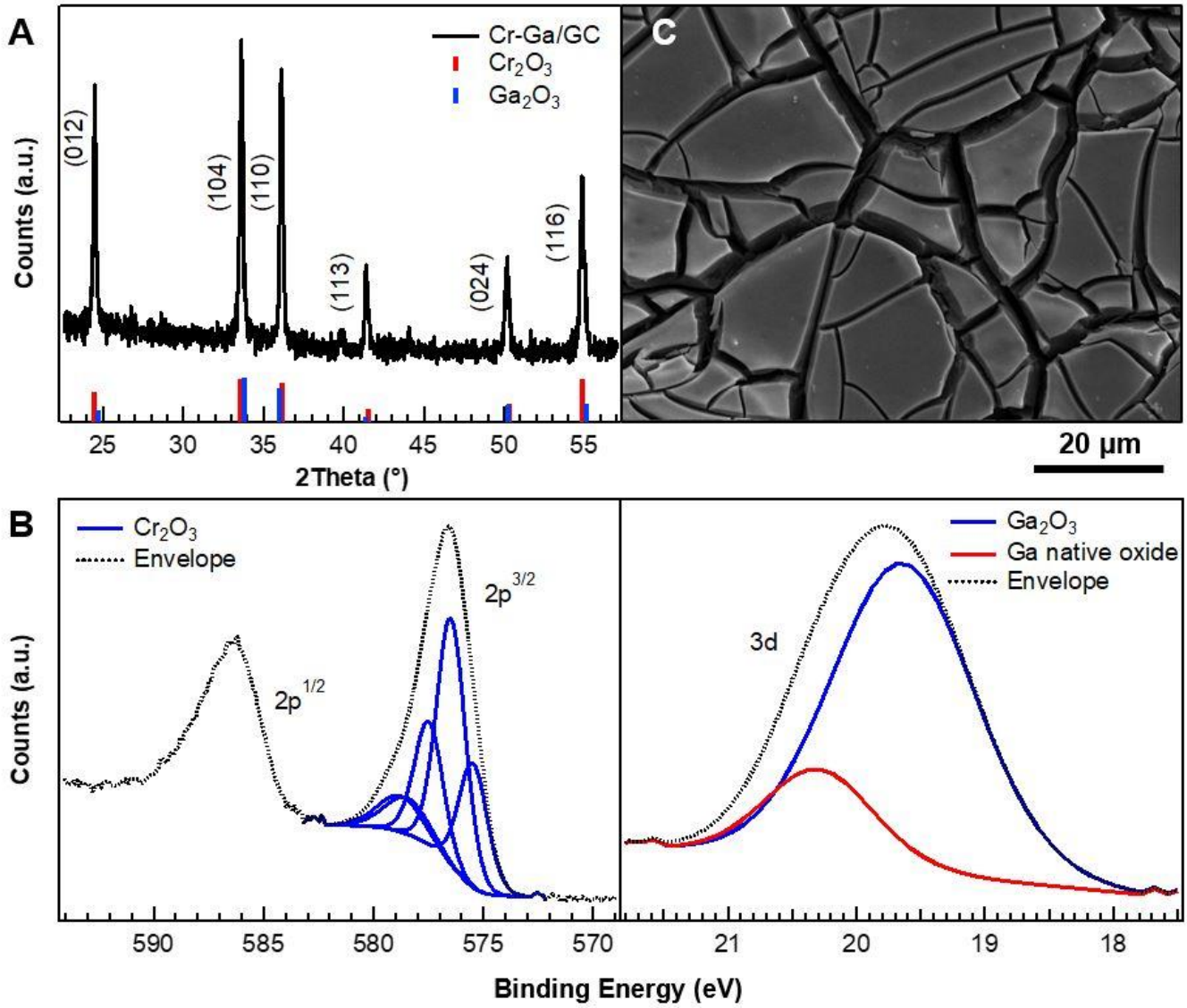

Figure 1. Materials characterization of Cr-Ga thin film on glassy carbon. (A) XRD pattern of Cr-Ga referenced to Cr_2O_3 (PDF 00-038-1479) and Ga_2O_3 (PDF 01-074-1610). (B) Fitted XPS spectra of Cr (left) and Ga (right), indicating that the surface is made up of metal oxides. Peaks are referenced to adventitious carbon at 284.5 eV (not shown). (C) SEM image of Cr-Ga comprising discontinuous platelets on the solid support surface, obtained using a 10 keV electron beam and 14.2 mm working distance.

one treated with HCl and the other untreated prior to calcium bromide addition; the difference in mass was attributed to calcium carbonate, which was then calculated as a percentage of the total CO_2 in solution (based on the electrolyte volume unique to each experiment. Calcium carbonate was also examined by IR spectroscopy. Experimental calcium oxalate and calcium carbonate samples were compared to control compounds made by combining calcium bromide and either oxalic acid or K_2CO_3 in aqueous solution.

Headspace samples were analyzed by gas chromatography for gaseous products. CO was measured using a HP6890 Gas Chromatograph fitted with a Molsieve 5A PLOT capillary column (Agilent) and TCD. The sampling method was a 5-min, 60 °C isotherm with He flow gas. An SRI 8610C Gas Chromatograph with Ar flow, which also used a Molsieve column and TCD, was run for a 7-min isotherm at 80 °C to detect H_2. CO and H_2 were quantified using 30-point calibration curves having R^2 values ≥ 0.99. The headspace was also sampled following $^{13}CO_2$ electrolyses using a KBr-terminated gas cell and Nicolet iS50 FT-IR Spectrometer with 1 cm^{-1} resolution; this confirmed that the CO product was derived from CO_2. Faradaic efficiencies for all products, gaseous and liquid, were calculated based on the charge passed during each experiment as well as the product quantities determined by gas chromatography, ^{1}H-NMR, or calcium bromide precipitation. Catalytic efficiencies were calculated based on the following equation established by Pander *et al.*[25]:

$$\text{Catalytic efficiency} = \frac{\text{Faradaic efficiency}}{\left(1+\frac{\text{overpotential}}{E^{o'}_{\text{product}}}\right)} \times 100\% \qquad \textit{Eqn. 1}$$

3. RESULTS AND DISCUSSION

3.1 Synthesis, characterization, and electrochemistry of Cr-Ga on glassy carbon

Thin films of Cr-Ga (3:1 ratio) on glassy carbon solid supports were synthesized using a drop-casting and thermal reduction method adapted from Torelli *et al.*[26] Powder X-ray diffraction (XRD; Figure 1A) coupled with energy-dispersive X-ray spectroscopy (SEM/EDX; Figure S2) suggested that the bulk films were comprised of Cr_2O_3 and Ga_2O_3 in a 3:1 ratio. High-resolution transmission electron microscopy (HR-TEM) with nano-EDX capability indicated that, compositionally, a single oxide phase having 3:1 metal stoichiometry was present. Taken together, the XRD and HR-TEM data allow assignment of this material as an alloy of Cr_2O_3 and Ga_2O_3.

The bulk film was further analyzed by performing Ar-ion bombardment in the analysis chamber of an X-ray photoelectron spectrometer over multiple 10-s intervals. In this process, the top layers of the film were removed, exposing the bulk material as the new "surface" and allowing for further confirmation of a 3:1 Cr_2O_3:Ga_2O_3 composition (Figure S3). Without Ar-ion bombardment, X-ray photoelectron spectroscopy (XPS) suggests that surface compositions were also comprised of Cr[27–29] and Ga[30] oxides (Figure 1B), consistent with the bulk. Scanning electron microscopy (SEM; Figure 1C) indicated that Cr-Ga films consisted of discontinuous platelets scattered across the glassy carbon surface, not unlike alternative thin film systems similarly synthesized.[26,31]

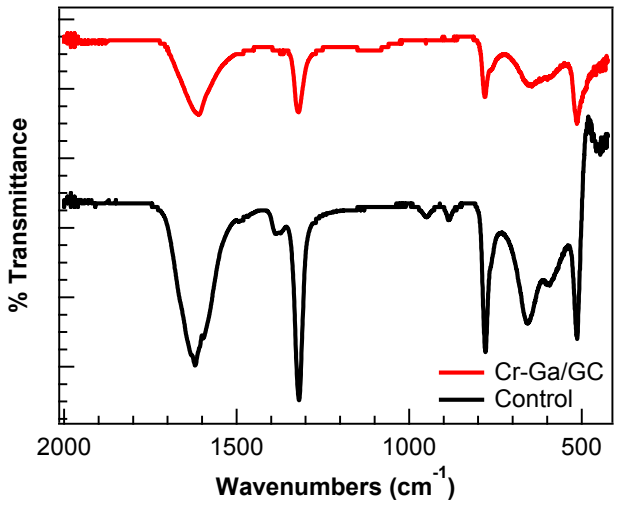

Figure 2. IR spectrum of calcium oxalate derived from Cr-Ga-mediated electrolysis (red), confirming that oxalate is a CO_2 reduction product. To obtain calcium oxalate, electrolysis samples were treated with calcium bromide, resulting in precipitation of the oxalate salt. Control experiments in which commercial oxalic acid was isolated from aqueous solution using calcium bromide yielded an identical IR spectrum (black).

Following cyclic voltammetry experiments, which indicated modest current enhancement under CO_2 saturation compared to Ar (Figure S4), initial bulk electrolysis experiments were conducted using a Pt mesh counter electrode and 0.1 M KCl electrolyte (pH 4 after CO_2 saturation). Applying a potential of –1.38 V vs. Ag/AgCl to an electrochemical cell purged with $^{13}CO_2$ induced generation of CO and H_2, sampled by gas chromatography, as well as oxalate, formate, and methanol, detected in the liquid phase by ^{1}H- and ^{13}C-NMR (Figures S5, S6A). Specifically, oxalate was assigned as the high-intensity ^{13}C-NMR peak at 161 ppm that overshadowed formate, methanol, and residual CO_2 signals (Figure S6A). To confirm this product assignment, a sample of the electrolyzed solvent (treated with HCl to remove carbonate, if present) was mixed with aqueous calcium bromide, causing precipitation of a white solid (Figure S6B), which was isolated by vacuum filtration and examined by infrared (IR) spectroscopy (Figure 2). Only IR transitions associated with calcium oxalate were observed.[32–34]

3.2 Optimizing oxalate generation by manipulating electrochemical conditions

To optimize the Cr-Ga system for oxalate production, pH and potential dependence studies were undertaken. Gravimetric determination of oxalate is well established[35,36] and was found to be quantitative in the present study when a 1 M calcium bromide solution was added to post-electrolysis samples. Standard curves were employed for quantifying CO/H_2 and formate/methanol using gas chromatography and ^{1}H-NMR, respectively.

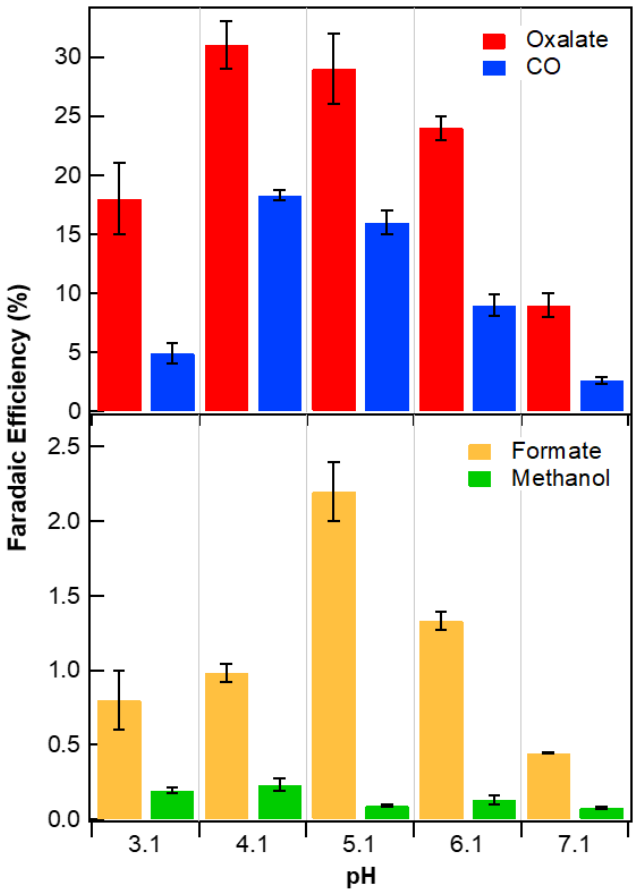

Figure 3. pH dependence of Faradaic efficiencies for carbon-containing products. Experiments were performed at –1.38 V vs. Ag/AgCl using CO_2-saturated 0.1 M KCl buffered with $KHCO_3$ (pH > 4) or adjusted with HCl (pH < 4). Differences in oxalate generation ability from pH 4.1–6.1 were minimal.

All pH-varying experiments were conducted at an applied potential of –1.38 V vs. Ag/AgCl and used CO_2-saturated KCl electrolyte (buffered with $KHCO_3$ for pH > 4; adjusted with HCl for pH < 4; 0.1 M concentration). As shown in Figure 3 and listed in Table S1, the Cr-Ga system appears only somewhat sensitive to solution pH, since statistically equivalent

oxalate Faradaic efficiencies were achieved at pH 4.1 and 5.1, while pH 6.1 yielded slightly inferior results. Markedly lower Faradaic efficiencies at pH 7.1 hinted that HCO_3^-, detected in trace amounts by gravimetric analysis even in non-buffered experiments, is not involved in oxalate production;[37] its presence is rationalized in later sections. During electrolysis, charge balance was achieved by H_2 generation (Figure S7).

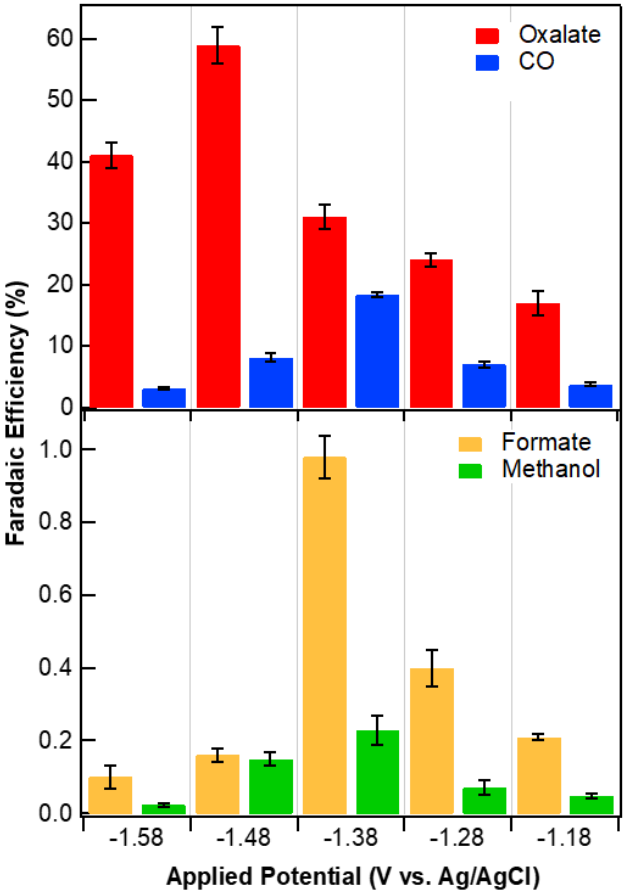

Figure 4. Potential dependence of Faradaic efficiencies for carbon-containing products. Experiments used pH 4.1, 0.1 M KCl electrolyte. Optimal oxalate production was achieved at –1.48 V vs. Ag/AgCl.

Subsequent experiments utilized CO_2-saturated, pH 4.1 KCl, because this pH maximized total Faradaic efficiency for carbon-containing products compared to H_2. Bulk solution pH consistently rose to 4.5–5.0 by the end of electrolysis (when initial pH = 4.1) but, as shown in Figure 3, maximum oxalate Faradaic efficiencies are still achieved at these final pH values. Potential dependence experiments at pH 4.1 resulted in oxalate formation at all potentials examined between –1.18 V and –1.58 V vs. Ag/AgCl. Notably, the potentials in this window are more positive than the thermodynamic potential required to achieve the one-electron reduction of CO_2 to $CO_2^{\bullet-}$, indicating that $CO_2^{\bullet-}$ is not generated in this oxalate-forming process. The product Faradaic efficiencies achieved during potential dependence experiments are displayed in Figure 4 and listed in Table S2. An electrode potential of –1.48 V vs. Ag/AgCl was determined to be optimal for oxalate production.

A cell employing 0.1 M KCl (pH 4.1) at a potential of –1.48 V vs. Ag/AgCl generated Faradaic efficiencies for oxalate, CO, formate, and methanol of 59 ± 3%, 8.1 ± 0.7%, 0.16 ± 0.02%, and 0.15 ± 0.02%, respectively, over a 4-h period. These values correspond to catalytic power efficiencies, as defined by Pander *et al.*,[25] of 22% (oxalate), 3.2% (CO), 0.054% (formate), and 0.045% (methanol). Current vs. time curves exhibited stable current densities at 8–10 mA/cm^2 (Figure 5), calculated based on geometric surface area of the electrode.

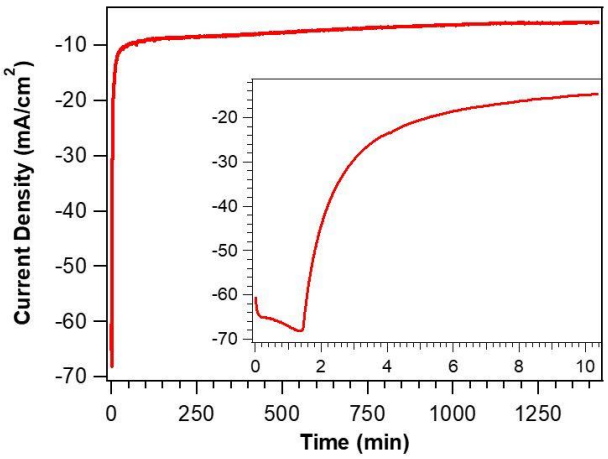

Figure 5. Sample current vs. time plot recorded during Cr-Ga on glassy carbon-mediated electrolysis at –1.48 V vs. Ag/AgCl. Inset depicts the first 10 min of electrolysis, where a current spike prior to the 2-min mark likely corresponds to reduction of native Ga surface oxides. KCl (pH 4.1) was used as the electrolyte and Pt mesh as the counter electrode.

To determine the overpotential for CO_2 reduction at the Cr-Ga electrode, it is critical to consider the protonation state of the oxalate being generated. The pK_a values of diprotic oxalic acid are reported to be 1.25 and 4.14 for the first and second proton dissociations, respectively.[38] All literature reports that reduce CO_2 to oxalate in organic or low-proton-activity solvents, produce the oxalate dianion. The Cr-Ga system, which yields maximum oxalate Faradaic efficiencies around pH 4.1, generates a combination of monoanionic and dianionic oxalate.[39] As shown in Text S1, relative quantities of the monoanionic and dianionic species were calculated at each pH tested, indicating that, at pH 4.1, the quantity of oxalate monoanion slightly exceeds that of the dianion. This product distribution is unique—further distinguishing Cr-Ga from prior reports of oxalate formation—and adds appeal to the system because protonated oxalates are more favorable industrial targets than their fully anionic analog.[40,41] Based on this ~50/50 product distribution, E_R° for the Cr-Ga-based electrochemical reaction was approximated to be halfway between the E_R° values for CO_2 reduction to the monoanionic and dianionic species, or –0.58 V vs. NHE (–0.79 V vs. Ag/AgCl; see Text S2 for calculations). Accordingly, maximum oxalate Faradaic efficiencies were achieved at 690 mV overpotential (operating potential = –1.48 V vs. Ag/AgCl), while the onset of oxalate production was noted at overpotentials as low as 390 mV (operating potential = –1.18 V vs. Ag/AgCl).

Post-electrolysis materials characterization suggested that Cr-Ga continued to be chemically and physically stable. XPS analysis revealed that surface-confined Cr and Ga both remained predominantly oxidized (Figure S8A), as only Ga's native surface oxides were reduced off during the first few minutes of electrolysis (see Figure 5). SEM imaging indicated that the thin film incurred only slight erosion at platelets' edges during electrolysis (Figure S8B), while EDX showed that the 3:1 stoichiometry of metal oxides was maintained (Figure S8C). While maximum Faradaic efficiencies were achieved within the first 24 h of electrolysis, the Cr-Ga/glassy carbon electrode could produce oxalate continuously for at least 10 days (the longest time period studied) at Faradaic efficiencies ≥ 40%, suggesting an attractive catalytic lifetime (Figure S9).

3.3 The electrocatalytic ratio of Cr and Ga oxides

Compared to literature systems, Cr-Ga employs anomalous conditions to achieve high oxalate Faradaic efficiencies from CO_2, inviting questions about the roles of the metal oxides within the catalyst. To address this question, we first examined single-metal oxide films as electrocatalysts. At –1.48 V vs. Ag/AgCl (pH 4.1 KCl), neither Cr_2O_3 nor Ga_2O_3 films alone could produce oxalate from CO_2, confirming the importance of having both oxides present. Films of Cr_2O_3 on glassy carbon generated modest amounts of CO, formate, and methanol from CO_2, while the activity of Ga_2O_3 films was dominated by CO production at around 40% Faradaic efficiency. These results for the single-metal oxide thin films vary slightly from those published for their bulk metal analogs.[42,43] Both single-metal species remained oxidized after electrochemical testing.

Following electrolysis using plain Ga_2O_3 films, it was noted that about 20% of the aqueous CO_2 had converted to HCO_3^-, identifiable both in solution and on the electrode surface by XPS (Figures S10, S11). Because CO_2 and carbonate species exist in acid-base equilibrium in aqueous solution, it appears that Ga_2O_3 shifted this equilibrium toward HCO_3^-. To further examine the acid-base equilibrium of CO_2 in the presence of Ga_2O_3, a 0.5-g sample of Ga_2O_3 powder was added to a beaker of CO_2-purged water (~30 mL), and a bulk solution pH change of +0.4 pH unit was recorded within 30 min. With a pK_a of 8.1, Ga_2O_3 surface hydroxide groups should create a basic local environment, shifting the CO_2/HCO_3^- equilibrium (pK_a = 6.4) toward HCO_3^- and subsequently impacting bulk pH. This phenomenon introduces the possibility that the active redox species is HCO_3^-; however, supplying the Cr-Ga system with 30 mM HCO_3^- instead of CO_2 failed to result in oxalate production, confirming that the active species is, in fact, CO_2. Given that the CO_2/HCO_3^- equilibrium involves relatively slow kinetics, the reactant could become kinetically trapped in the HCO_3^- form, stoichiometrically limiting the rate of charge transfer to CO_2.

Because Ga_2O_3 facilitates this detrimental equilibrium shift yet needs to be present in the alloy to obtain efficient oxalate production, an optimal Cr_2O_3:Ga_2O_3 stoichiometry must exist. To determine this ratio, a range of stoichiometries spanning from 100% Cr_2O_3 to 100% Ga_2O_3 were synthesized as thin films on glassy carbon and analyzed for their performance as CO_2 reduction electrocatalysts via bulk electrolysis. All experiments were conducted at –1.48 V vs. Ag/AgCl in 0.1 M KCl (pH 4.1) for comparison to the optimized oxalate outcome for Cr-Ga. Results are presented in Figure 6 and tabulated in Table S3. CO and formate quantities generally amplified as Ga_2O_3 percentage increased and, as expected, ratios favoring Ga_2O_3 corresponded to more HCO_3^- detected post-electrolysis. Cr_2O_3-rich stoichiometries resulted in lower overall quantities of non-oxalate, carbon-containing products compared to Ga_2O_3-rich variants, but Faradaic efficiencies for CO reached their lowest values at the highest percentages of Cr_2O_3. Importantly, the highest Faradaic efficiency for oxalate was obtained at the original 3:1 stoichiometry, which appears to provide just enough Ga_2O_3 for oxalate generation purposes while minimizing the interfacial pH shift that edges the CO_2 equilibrium toward HCO_3^-.

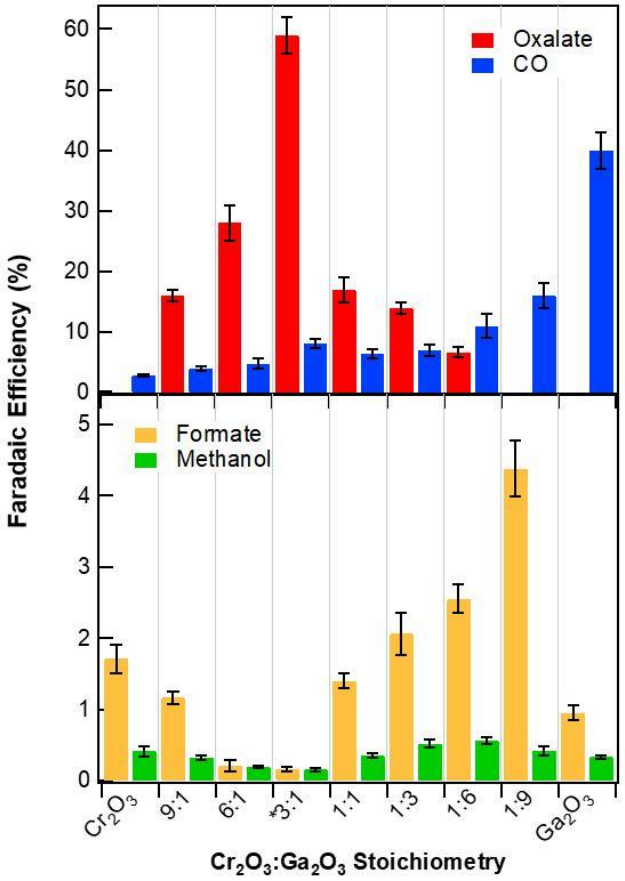

Figure 6. Faradaic efficiencies achieved for carbon-containing products based on Cr_2O_3:Ga_2O_3 stoichiometry, suggesting that 3:1 is the optimal (*) ratio for oxalate generation. CO generation is favored by Ga_2O_3-rich stoichiometries and hindered by Cr_2O_3 analogs. Oxalate and formate exhibit inverse production trends. Electrolyses were performed at –1.48 V vs. Ag/AgCl in 0.1 M KCl (pH 4.1).

3.4 The roles of CO and methanol in oxalate generation

Ultimately, the Cr-Ga catalyst demonstrates that CO_2 electroreduction to oxalate can occur both in protic environments and at much lower applied potentials than previously recognized. At the potentials studied here, ranging from 530 to 930 mV more positive than the E_R° required for $CO_2^{\bullet-}$ generation, CO_2 reduction to oxalate must occur via a $CO_2^{\bullet-}$-independent pathway. This suggests that one or more of the C1 products observed in the electrochemical

Table 1. Products Generated Based on Electrolyte Cation Identity.[†]

Electrolyte cation	Faradaic efficiency (%)[‡]			
	Oxalate	*CO*	*Formate*	*Methanol*
Li^+	48 ± 5	13.8 ± 0.7	0.13 ± 0.03	0.09 ± 0.02
K^+	59 ± 3	8.1 ± 0.7	0.16 ± 0.02	0.15 ± 0.02
NH_4^+	45 ± 4	6.4 ± 0.5	0.20 ± 0.04	0.16 ± 0.04
Cs^+	0	3.6 ± 0.5	4.2 ± 0.3	0.21 ± 0.03
TMA^+	0	1.8 ± 0.5	7.7 ± 0.4	0.95 ± 0.07
Ca^{2+}	0	3.7 ± 0.6	5.1 ± 0.4	0.52 ± 0.03

[†]Electrolyses were performed at –1.48 V vs. Ag/AgCl in 0.1 M electrolyte solution (CO_2-saturated, pH 4.1), where Cl^- was the counter anion.

[‡]Standard deviation based on the average of three trials using different Cr-Ga electrodes.

cell serve as oxalate precursors. To investigate this possibility, electrolysis experiments were performed by replacing the CO_2 feedstock with CO, formate, methanol, or combinations of these carbon-containing compounds. Single-feedstock experiments failed to yield oxalate, although use of either CO or formate as the reactant resulted in trace quantities of methanol. Importantly, electrolysis experiments conducted using a combined feedstock of ^{13}CO and 15 mM methanol (rather than CO_2) did produce oxalate, as confirmed by precipitation with calcium bromide as well as ^{13}C-NMR (Figure S12A). This ^{13}CO experiment, which used ^{12}C-methanol, also verified that the carbon atoms of the oxalate product were derived from CO.

The opposite labeling experiment, using ^{12}CO and ^{13}C-methanol, was also undertaken, resulting in no ^{13}C-NMR signal even though calcium oxalate was precipitated out of solution (Figure S12B). Therefore, methanol's carbon atom is not incorporated into the product, despite the fact that the system requires both methanol and CO to produce oxalate. Further, when the typical CO_2-saturated electrolyte (0.1 M KCl) was adjusted to contain 15 mM methanol prior to electrolysis (–1.48 V vs. Ag/AgCl), normal quantities of oxalate were achieved, but 5 M methanol yielded only trace amounts of product. Substituting methanol with either high or low concentrations of acetonitrile, ethanol, or isopropanol resulted in the same effects on oxalate production. This could be attributed to alterations in water's hydrogen bonding network at or near the catalyst surface facilitated by non-trivial concentrations of organic solvent in the otherwise aqueous solution.[44,45]

To test this hypothesis, Cr-Ga-mediated CO_2 electrolysis was performed using 0.1 M KCl in D_2O, which exhibits different hydrogen bonding character compared to H_2O.[46] In these experiments, oxalate was not detectable, while CO was generated at 17 ± 2% Faradaic efficiency, approximately double its value in H_2O. It appears that oxalate yields suffer when the hydrogen bonding network is significantly altered, but minor amounts of solvent—like the quantity of methanol generated by Cr-Ga—are required for oxalate synthesis. Taken together, these observations point to a strong influence of hydrogen bonding at the Cr-Ga surface. If this is true, one might expect that addition of a hydrogen bond-breaking agent, like the organics used in previous experiments, would fail to recover oxalate generation capacity in D_2O, whose hydrogen bonding is already "disrupted" (i.e., compared to H_2O). Indeed, oxalate was not produced in a control experiment adding 15 mM methanol to D_2O-based electrolyte, further supporting the system's sensitivity to hydrogen bonding environment.

3.5 The nature of Cr-Ga surface sites active in CO_2 reduction

Notably, the reactant experiments that initially pointed to oxalate-generating roles for CO and methanol did not implicate an important role for formate, which has been indicated as a competitor of oxalate production in the literature.[8] With a Cr-Ga electrode, use of a formate feedstock resulted in only trace amounts of methanol and failed to generate oxalate. This result suggested that distinct active sites might exist for generation of formate and CO-derived products, including oxalate. Further support for this prediction was provided by electrolyte dependence studies. While experiments varying the electrolyte anion (i.e., KCl, KBr, KI, K_2SO_4, and KH_2PO_4) failed to exhibit significant differences in the distribution of products, a stark dependence was noted when varying the electrolyte cation.

Use of LiCl or NH_4Cl electrolytes (0.1 M) and –1.48 V vs. Ag/AgCl applied potential resulted in similar product distributions and efficiencies as those recorded for KCl. However, analogous experiments using CsCl, $(CH_3)_4NCl$ ((TMA)Cl), and $CaCl_2$ electrolytes failed to generate any detectable quantities of oxalate, and CO Faradaic efficiencies were also reduced. (TMA)Cl supporting electrolyte increased the Faradaic efficiency of formate to 7.7 ± 0.4%, compared to the 0.16 ± 0.02% value achieved using optimal oxalate-generating conditions (0.1 M KCl). These cation-dependence results are summarized in Table 1. Furthermore, Cr-Ga electrodes previously used in (TMA)Cl experiments did not regain their oxalate-generating ability when re-introduced into a KCl-containing electrolyte. This KCl electrolyte was subjected to ^1H-NMR after electrolysis, and the resultant spectrum exhibited an overwhelming signal from TMA^+, which must have come from the Cr-Ga surface. TMA^+ had therefore chemisorbed to the catalyst during prior electrolyses, likely

contributing to inhibition of oxalate generation in those and subsequent experiments. Formate generation remained higher than usual in these trials.

Exacerbation of formate production when oxalate generation is suppressed further supports the proposal that at least two surface active sites are present in the Cr-Ga catalyst: one for CO and CO-derived productions and a second for formate. Moreover, chemisorption of TMA^+ onto the Cr-Ga surface suggests that a surface anion is present, while lack of oxalate production in the presence of cations having few waters of hydration (TMA^+ and Cs^+) or strong anion-binding capacity (Ca^{2+}) hints that this surface anion is critical to CO/oxalate generation. To probe this theory, we treated the Cr-Ga system (0.1 M KCl, –1.48 V vs. Ag/AgCl) with 15 mM NaCN prior to electrolysis, anticipating that the Lewis-basic, anionic CN^- ligand would bind specifically to a Lewis-acidic, non-anionic surface site. Indeed, after performing electrolysis with this modified system, CO, oxalate, and methanol were detected in typical yields, while no formate was produced. Thus, it appears that the CN^- ligates the formate-generating active site, simultaneously demonstrating that this site is (A) chemically distinct from the CO-generating site and (B) not anionic in character. This experiment, combined with the cation-dependence data, strongly suggests that Cr-Ga contains two types of electrocatalytic surface sites for CO_2 reduction: an anionic site leading to CO-derived products and a non-anionic site that produces formate (Figure 7).

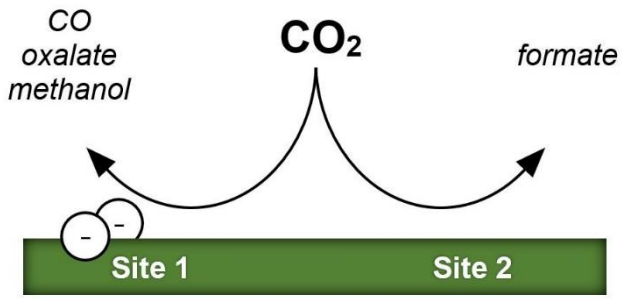

Figure 7. Schematic representation of proposed Cr-Ga surface sites active in electrochemical CO_2 reduction. A surface anion facilitates generation of CO and CO-derived products (including oxalate), while a separate site produces formate, which is not associated with the oxalate-generation pathway.

4. CONCLUSION

The ability of the Cr-Ga thin film on glassy carbon to generate oxalate from CO_2 in acidic aqueous electrolyte at 690 mV overpotential makes it a landmark example of heterogeneous CO_2 electroreduction, in part because the electrochemical conditions employed generate an equilibrium mixture of oxalate and its monoanionic form. More importantly, the current work demonstrates a major reduction in system overpotential compared to prior work in aprotic electrolytes. Furthermore, the maximum Faradaic efficiency of 59 ± 3% reported here for a two-carbon CO_2 reduction product is competitive with the best reported copper systems,[47–51] which are frequently considered state-of-the-art yet cannot produce oxalate as a product.[52]

With optimal electrolysis conditions of pH 4.1 aqueous KCl and –1.48 V vs. Ag/AgCl, the pathway used to generate oxalate by the Cr-Ga system cannot include a $CO_2^{\bullet-}$ intermediate. Instead, a surface anion is instrumental in reducing CO_2 to CO, which subsequently reacts to form oxalate. Interfering with the catalyst system by poisoning its critical surface anion sites or adequately disrupting the aqueous hydrogen bonding environment inhibits oxalate generation. Formate production, which occurs at a separate site, can be eliminated in the presence of a strong, anionic ligand, which interacts with the surface at non-anionic Lewis acid locations. Altering the percent composition of either Cr_2O_3 or Ga_2O_3 away from the optimal 3:1 stoichiometry decreases production of the CO intermediate or increases the quantity of unreactive HCO_3^- derived from CO_2.

High oxalate Faradaic efficiencies and initial lifetime studies exceeding 10 days of continuous use make Cr-Ga thin films on glassy carbon electrodes a promising CO_2 electroreduction system. The fact that Cr-Ga achieves an oxalate end product using aqueous solution, atmospheric pressure, and CO_2 starting material invites questions about whether, with additional studies, Cr-Ga could be a candidate catalyst for industrial oxalate production. As such, the chemistry facilitated by the Cr-Ga electrode lends real credibility to the goal of using electroreduction to turn society's problem of excess CO_2 into profitable future opportunities.

ASSOCIATED CONTENT

Supporting Information: Sample calculations, additional materials characterization, cyclic voltammetric data, NMR spectra, charge-balance plots, additional figures and tables.

The Supporting Information is available free of charge via the Internet at http://pubs.acs.org.

AUTHOR INFORMATION

Corresponding Author

*bocarsly@princeton.edu

Author Contributions

A.R.P. carried out all experiments. A.B.B. supervised the project. Both authors contributed to experiment design, interpretation of results, and manuscript preparation.

Notes

A.R.P. and A.B.B. of Princeton University have filed International Patent Application No. PCT/US2018/050016 regarding binary alloys and oxides thereof for electrocatalytic reduction of carbon dioxide.

ACKNOWLEDGMENT

The authors thank Ms. Jessica Frick for assistance obtaining XRD measurements, Mr. Steven Tignor for informative discussions, and Dr. Istvan Pelczer for support collecting ^{13}C-NMR spectra. The authors acknowledge the National Science Foundation for financially supporting this work under Grant No. CHE-1800400. Additionally, ARP acknowledges funding from the National Science Foundation Graduate Research Fellowship Program under Grant No. DGE-1148900. Any opinions, findings, and conclusions or recommendations expressed in this material are those of the authors and do not necessarily reflect the views of the National Science Foundation.

ABBREVIATIONS

Cr-Ga, 3 Cr_2O_3:1 Ga_2O_3; XRD, X-ray diffraction; EDX, energy-dispersive X-ray spectroscopy; HR-TEM, high-resolution transmission electron microscopy; XPS, X-ray photoelectron spectroscopy; SEM, scanning electron microscopy; NMR, nuclear magnetic resonance spectroscopy; IR, infrared; TMA, tetramethylammonium.

REFERENCES

(1) Dlugokencky, E.; Tans, P. *Trends in Atmospheric Carbon Dioxide*; Global Monitoring Division; Global Greenhouse Gas Reference Network; NOAA/Earth System Research Laboratory, 2016.

(2) *Climate Change Impacts in the United States: The Third National Climate Assessment*; U.S. Global Change Research Program, 2014; pp 69–256.

(3) Aresta, M.; Dibenedetto, A. The Contribution of the Utilization Option to Reducing the CO_2 Atmospheric Loading: Research Needed to Overcome Existing Barriers for a Full Exploitation of the Potential of the CO_2 Use. *Catal. Today* **2004**, *98*, 455–462.

(4) Liu, J.; Yang, W.; Li, L.; Wang, W.; Zhang, L.; Song, H. Method for the Production of Ethylene Glycol. US 8962895 B2.

(5) Yang, W.; Liu, J.; Wang, W.; Kuai, J. Method for Producing Ethylene Glycol from Oxalate through the Fluidized Bed Catalytic Reaction. US 20130331617 A1.

(6) Pang, K.; Kotek, R.; Tonelli, A. Review of Conventional and Novel Polymerization Processes for Polyesters. *Prog. Polym. Sci.* **2006**, *31*, 1009–1037.

(7) *Standard Potentials in Aqueous Solution*; Bard, A. J., Parsons, R., Jordan, J., Eds.; IUPAC, Physical and Analytical Chemistry Divisions, Marcel-Dekker: New York, 1985.

(8) Amatore, C.; Saveant, J. M. Mechanism and Kinetic Characteristics of the Electrochemical Reduction of Carbon Dioxide in Media of Low Proton Availability. *J. Am. Chem. Soc.* **1981**, *103*, 5021–5023.

(9) Gennaro, A.; Isse, A. A.; Severin, M.-G.; Vianello, E.; Bhugun, I.; Savéant, J.-M. Mechanism of the Electrochemical Reduction of Carbon Dioxide at Inert Electrodes in Media of Low Proton Availability. *J. Chem. Soc., Faraday Trans.* **1996**, *92*, 3963–3968.

(10) Rudolph, M.; Dautz, S.; Jäger, E.-G. Macrocyclic [N_4^{2-}] Coordinated Nickel Complexes as Catalysts for the Formation of Oxalate by Electrochemical Reduction of Carbon Dioxide. *J. Am. Chem. Soc.* **2000**, *122*, 10821–10830.

(11) Senthil Kumar, R.; Senthil Kumar, S.; Anbu Kulandainathan, M. Highly Selective Electrochemical Reduction of Carbon Dioxide Using Cu Based Metal Organic Framework as an Electrocatalyst. *Electrochem. Commun.* **2012**, *25*, 70–73.

(12) Eggins, B. R.; Brown, E. M.; McNeill, E. A.; Grimshaw, J. Carbon Dioxide Fixation by Electrochemical Reduction in Water to Oxalate and Glyoxalate. *Tetrahedron Lett.* **1988**, *29*, 945–948.

(13) Eggins, B. R.; Bennett, E. M.; McMullan, E. A. Voltammetry of Carbon Dioxide. Part 2. Voltammetry in Aqueous Solutions on Glassy Carbon. *J. Electroanal. Chem.* **1996**, *408*, 165–171.

(14) Ang, P. G. P.; Sammells, A. F.; Morduchowitz, A. Means and Method for Reducing Carbon Dioxide to Provide an Oxalate Product. US 4595465 A.

(15) Becker, J. Y.; Vainas, B.; Eger, R.; Kaufman, L. Electrocatalytic Reduction of CO_2 to Oxalate by Ag^{II} and Pd^{II} Porphyrins. *J. Chem. Soc., Chem. Commun.* **1985**, 1471–1472.

(16) Kushi, Y.; Nagao, H.; Nishioka, T.; Isobe, K.; Tanaka, K. Oxalate Formation in Electrochemical CO_2 Reduction Catalyzed by Rhodium-Sulfur Cluster. *Chem. Lett.* **1994**, 2175–2178.

(17) Kushi, Y.; Nagao, H.; Nishioka, T.; Isobe, K.; Tanaka, K. Remarkable Decrease in Overpotential of Oxalate Formation in Electrochemical CO_2 Reduction by a Metal-Sulfide Cluster. *J. Chem. Soc., Chem. Commun.* **1995**, 1223–1224.

(18) Angamuthu, R.; Byers, P.; Lutz, M.; Spek, A. L.; Bouwman, E. Electrocatalytic CO_2 Conversion to Oxalate by a Copper Complex. *Science* **2010**, *327*, 313–315.

(19) Lan, J.; Liao, T.; Zhang, T.; Chung, L. W. Reaction Mechanism of Cu(I)-Mediated Reductive CO_2 Coupling for the Selective Formation of Oxalate: Cooperative CO_2 Reduction to Give Mixed-Valence $Cu_2(CO_2^{\bullet-})$ and Nucleophilic-like Attack. *Inorg. Chem.* **2017**, *56*, 6809–6819.

(20) Ooka, H.; Figueiredo, M. C.; Koper, M. T. M. Competition between Hydrogen Evolution and Carbon Dioxide Reduction on Copper Electrodes in Mildly Acidic Media. *Langmuir* **2017**, *33*, 9307–9313.

(21) There is one literature report that suggests that oxalate can be generated in ultra-low-proton-activity aqueous electrolyte ($[a_H^+]=10^{-10}$).[12,13] However, this 30-year old report has not been reproduced and lacks the minimum acceptable control experiments.

(22) Gressin, J. C.; Michelet, D.; Nadjo, L.; Savéant, J.-M. Electrochemical Reduction of Carbon Dioxide in Weakly Protic Medium. *Nouv. J. Chim.* **1979**, *3*, 545–554.

(23) Benson, E. E.; Kubiak, C. P.; Sathrum, A. J.; Smieja, J. M. Electrocatalytic and Homogeneous Approaches to Conversion of CO_2 to Liquid Fuels. *Chem. Soc. Rev.* **2009**, *38*, 89–99.

(24) See, for example: (A) A. A. Noyes and E. H. Swift, "Qualitative Analysis of Inorganic Substances," pg 361, The MacMillan Company, New York (1945); (B) C. J. L. Baker, "The Determination of Oxalates in Fresh Plant Material," *Analyst*, (1952) 77, 340-344.

(25) Pander, J. E.; Fogg, A.; Bocarsly, A. B. Utilization of Electropolymerized Films of Cobalt Porphyrin for the Reduction of Carbon Dioxide in Aqueous Media. *ChemCatChem* **2016**, *8*, 3536–3545.

(26) Torelli, D. A.; Francis, S. A.; Crompton, J. C.; Javier, A.; Thompson, J. R.; Brunschwig, B. S.; Soriaga, M. P.; Lewis, N. S. Nickel–Gallium-Catalyzed Electrochemical Reduction of CO_2 to Highly Reduced Products at Low Overpotentials. *ACS Catal.* **2016**, *6*, 2100–2104.

(27) Aronniemi, M.; Sainio, J.; Lahtinen, J. Chemical State Quantification of Iron and Chromium Oxides Using XPS: The Effect of the Background Subtraction Method. *Surf. Sci.* **2005**, *578*, 108–123.

(28) Daulton, T. L.; Little, B. J. Determination of Chromium Valence over the Range Cr(0)-Cr(VI) by Electron Energy Loss Spectroscopy. *Ultramicroscopy* **2006**, *106*, 561–573.

(29) Biesinger, M. C.; Payne, B. P.; Grosvenor, A. P.; Lau, L. W. M.; Gerson, A. R.; Smart, R. S. C. Resolving Surface Chemical States in XPS Analysis of First Row Transition Metals, Oxides and Hydroxides: Cr, Mn, Fe, Co and Ni. *Appl. Surf. Sci.* **2011**, *257*, 2717–2730.

(30) Reddy, B. M.; Ganesh, I.; Reddy, E. P.; Fernández, A.; Smirniotis, P. G. Surface Characterization of Ga_2O_3–TiO_2 and V_2O_5/Ga_2O_3–TiO_2 Catalysts. *J. Phys. Chem. B* **2001**, *105*, 6227–6235.

(31) Paris, A. R.; Bocarsly, A. B. Ni–Al Films on Glassy Carbon Electrodes Generate an Array of Oxygenated Organics from CO_2. *ACS Catal.* **2017**, 6815–6820.

(32) Frost, R. L.; Yang, J.; Ding, Z. Raman Spectroscopy of Natural Oxalates–Implications for the Evidence of Life on Mars. *Chin. Sci. Bull.* **2003**, *48*, 1844–1852.

(33) Sofia, P. G.; Ionescu, I.; Rodica, G.; Anisoara, P. The Use of Infrared Spectroscopy in the Investigation of Urolithiasis. *Rev. Romana Med. Lab.* **2010**, *18*, 67–77.

(34) Peterson, K. I.; Pullman, D. P. Determining the Structure of Oxalate Anion Using Infrared and Raman Spectroscopy Coupled with Gaussian Calculations. *J. Chem. Ed.* **2016**, *93*, 1130–1133.

(35) Garside, J.; Brečević, L.; Mullin, J. W. The Effect of Temperature on the Precipitation of Calcium Oxalate. *J. Cryst. Growth* **1982**, *57*, 233–240.
(36) Erdey, L. Ca-Mg (Alkali Metals). In Gravimetric Analysis, Part II; Buzas, I., Ed.; Pergamon Press: New York, New York, 1965; Vol. 7.
(37) Banerjee, A.; Dick, G. R.; Yoshino, T.; Kanan, M. W. Carbon Dioxide Utilization via Carbonate-Promoted C–H Carboxylation. *Nature* **2016**, *531*, 215–219.
(38) Bjerrum, J.; Schwarzenbach, G.; Sillen, L. G. Stability Constants of Metal-Ion Complexes, with Solubility Products of Inorganic Substances, Part II; The Chemical Society: London, England, 1958; Vol. 7.
(39) Hernández, R. Á. H.; García, F. L.; Cruz, L. E. H.; Luévanos, A. M. Statistical Treatment of Bleaching Kaolin by Iron Removal. *J. Mex. Chem. Soc.* **2013**, *54*, 261–266.
(40) Carnahan, J. E.; Ford, T. A.; Gresham, W. F.; Grigsby, W. E.; Hager, G. F. Ruthenium-Catalyzed Hydrogenation of Acids to Alcohols. *J. Am. Chem. Soc.* **1955**, *77*, 3766–3768.
(41) Meurs, J. H. H. Method of Preparing Oxalic Acid. US2017370011 (A1), December 28, 2017.
(42) Hori, Y.; Wakebe, H.; Tsukamoto, T.; Koga, O. Electrocatalytic Process of CO Selectivity in Electrochemical Reduction of CO_2 at Metal Electrodes in Aqueous Media. *Electrochim. Acta* **1994**, *39*, 1833–1839.
(43) White, J. L.; Baruch, M. F.; Pander III, J. E.; Hu, Y.; Fortmeyer, I. C.; Park, J. E.; Zhang, T.; Liao, K.; Gu, J.; Yan, Y.; Shaw, T. W.; Abelev, E.; Bocarsly, A. B. Light-Driven Heterogeneous Reduction of Carbon Dioxide: Photocatalysts and Photoelectrodes. *Chem. Rev.* **2015**, *115*, 12888–12935.
(44) Alavi, S.; Takeya, S.; Ohmura, R.; Woo, T. K.; Ripmeester, J. A. Hydrogen-Bonding Alcohol-Water Interactions in Binary Ethanol, 1-Propanol, and 2-Propanol + Methane Structure II Clathrate Hydrates. *J. Chem. Phys.* **2010**, *133*, 074505.1-074505.8.
(45) Lam, R. K.; Smith, J. W.; Saykally, R. J. Hydrogen Bonding Interactions in Water-Alcohol Mixtures from X-Ray Absorption Spectroscopy. *J. Chem. Phys.* **2016**, *144*, 191103.
(46) Proteins in Solution and at Interfaces: Methods and Applications in Biotechnology and Materials Science; Ruso, J. M.; Pineiro, A., Eds.; John Wiley & Sons: New York, New York, 2013.
(47) Hori, Y.; Takahashi, I.; Koga, O.; Hoshi, N. Selective Formation of C2 Compounds from Electrochemical Reduction of CO_2 at a Series of Copper Single Crystal Electrodes. *J. Phys. Chem. B* **2002**, *106*, 15–17.
(48) Song, Y.; Peng, R.; Hensley, D. K.; Bonnesen, P. V.; Liang, L.; Wu, Z.; Meyer, H. M.; Chi, M.; Ma, C.; Sumpter, B. G.; Rondinone, A. J. High-Selectivity Electrochemical Conversion of CO_2 to Ethanol Using a Copper Nanoparticle/N-Doped Graphene Electrode. *ChemistrySelect* **2016**.
(49) Baturina, O.; Lu, Q.; Xu, F.; Purdy, A.; Dyatkin, B.; Sang, X.; Unocic, R.; Brintlinger, T.; Gogotsi, Y. Effect of Nanostructured Carbon Support on Copper Electrocatalytic Activity toward CO_2 Electroreduction to Hydrocarbon Fuels. *Catal. Today* **2017**, *288*, 2–10.
(50) Lum, Y.; Yue, B.; Lobaccaro, P.; Bell, A. T.; Ager, J. W. Optimizing C–C Coupling on Oxide-Derived Copper Catalysts for Electrochemical CO_2 Reduction. *J. Phys. Chem. C* **2017**, *121*, 14191–14203.
(51) Dinh, C.-T.; Burdyny, T.; Kibria, G.; Seifitokaldani, A.; Gabardo, C. M.; Edwards, J. P.; Luna, P. D.; Bushuyev, O. S.; Zou, C.; Quintero-Bermudez, R.; Pang, Y.; Sinton, D.; Sargent, E. H. CO_2 Electroreduction to Ethylene via Hydroxide-Mediated Copper Catalysis at an Abrupt Interface. *Science* **2018**, *360*, 783–787.
(52) Gattrell, M.; Gupta, N.; Co, A. A Review of the Aqueous Electrochemical Reduction of CO_2 to Hydrocarbons at Copper. *J. Electroanal. Chem.* **2006**, *594*, 1–19.

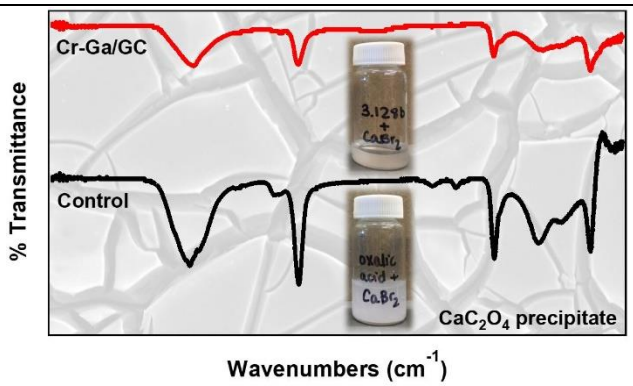
Cr-Ga/GC
Control
% Transmittance
3.129b
+
CaBr2
oxalic
acid +
CaBr2
CaC2O4 precipitate
Wavenumbers (cm-1)